RSC Advances

ROYAL SOCIETY OF CHEMISTRY

www.rsc.org/advances

RSC Advances

Cite this: DOI: 10.1039/c5ra00000x

www.rsc.org/advances

ARTICLE

Hydrothermal Syntheses, Structural Characterizations, and Magnetic Properties of Five MOFs Assembled From C_2-Symmetric Ligand of 1,3-Di((2',4'-dicarboxylphenyl)benzene with Various Coordination Modes

Liming Fan,[a,b] Weiliu Fan,[a] Bin Li,[b] Xian Zhao*[a] and Xiutang Zhang*[a,b]

Received (in XXX, XXX) Xth XXXXXXXXX 2015, Accepted Xth XXXXXXXXX 2015
DOI: 10.1039/c5ra00000x

ABSTRACT: Five new complexes, $[Ni(H_2DDB)(H_2O)_2(\mu_2\text{-}H_2O)]_n$ (**1**), $[Ni_{1.5}(DDB)(1,4\text{-bib})_{1.5}(H_2O)]_n$ (**2**), $\{[Ni_2(DDB)(1,3\text{-bib})_2(\mu_2\text{-}H_2O)]\cdot 2H_2O\}_n$ (**3**), $[Cu_2(H_2DDB)_2(1,4\text{-bib})_2]\cdot H_2O$ (**4**), and $\{[Cu_{1.5}(HDDB)(1,2\text{-bimb})]\cdot H_2O\}_n$ (**5**), have been synthesized by the solvothermal reaction of 1,3-di(2',4'-dicarboxylphenyl)benzene (H_4DDB) with nickel (II) or copper (II) salts in the presence of ancillary ligands of bis(imidazole) linkers (1,4-bib = 1,4-bis(1H-imidazol-4-yl)benzene, 1,3-bib = 1,3-bis(1H-imidazol-4-yl)benzene, and 1,2-bimb = 1,2-bis(imidazol-1-ylmethyl)benzene). Their structures have been determined by single-crystal X-ray diffraction analyses and further characterized by elemental analyses, IR spectra, powder X-ray diffraction (PXRD), and thermogravimetric (TG) analyses. In complex **1**, Ni^{II} ions are bridged by associated water molecules to form an interesting $[Ni(H_2DDB)(H_2O)_2(\mu_2\text{-}H_2O)]_n$ chain structure, which are further extended to a 3D supramolecular structure *via* the hydrogen bonds. In complex **2**, a novel 3D (3,3.6)-connected $(6^3)_4(6^5\cdot 8^8\cdot 10^2)$ net is generated from the synergistic effect of 1D $[Ni(1,4\text{-bib})]_n$ zigzag chains and 2D $[Ni_3(DDB)_2]_n$ bilayers. For complex **3**, with the employment of 1,3-bib bis(imidazole) linker instead of 1,4-bib, an unprecedented binuclear $\{Ni_2(COO)(\mu_2\text{-}H_2O)\}$ SBUs based 3D (3,6)-connected $(3\cdot 6\cdot 7)(3^2\cdot 4^3\cdot 5^4\cdot 6^3\cdot 7\cdot 8^2)$ net was obtained. Furthermore, once Ni^{II} ions was replaced by Cu^{II} ions, a paddle wheel $\{Cu_2(COO)_4\}$ SBUs based $[Cu_2(H_2DDB)(1,4\text{-bib})_2]$ (**4**) complex was formed. For complex **5**, 2D $[Cu_3(HDDB)_2]_n$ sheets are further linked by 1,2-bimb pillars to expand a paddle wheel $\{Cu_2(COO)_4\}$ SBUs based 3D architecture with 4-connected $(6^5\cdot 8)$-**cds** topology. Moreover, the magnetic properties of **1**, **3**, and **5** have been investigated.

Introduction

During the past decades, extensive experimental and theoretical efforts of metal organic frameworks (MOFs), has attracted a great deal of interest for their regulated and interesting structural topologies as well as their potential applications in the fields of photoluminescence, magnetism, catalysis, gas storage, conductivity, ion exchange, ferroelectricity, optoelectronic effect, nonlinear optics, and spin-transition behavior.[1-3] Such materials are constructed from metal ions as connected centers and multifunctional organic ligands as linkers usually.[4] In principle, the targeting assemblies with desired structural features and physicochemical properties greatly depend on the nature of the organic ligands and metal ions, among which the appropriate choice of well-designed organic building blocks and metal ions or clusters is one of the most effective ways.[5,6]

Despite the breathtaking achievements in this aspect, however, to predict and further accurately control the framework array of a given crystalline product still remain a considerable challenge at this stage. This mainly arises from the fact that the subtle assembled progress may be influenced by many intrinsic and external parameters, such as the different coordination preferences of metal ion, templating agents, metal-ligand ratio, pH value, counteranion, and number of coordination sites provided by organic ligands.[7-9]

Among the numerous organic ligands, the polycarboxylic acids and the N-donor ligands are favored for their strong coordinating ability, which could stabilize the packing architecture, including that of honeycomb, grid, T-shaped, ladder, diamondoid, and octahedral structures.[10,11] The ancillary ligands containing N-donor such as bipyridine have been used widely with polycarboxylates together to construct the desired structures.[12] For example, bipyridine linker as an N-donor ligand is beneficial to the syntheses of extended MOFs and can generate high dimensional structures owing to its simple bridging mode and strong coordination ability, while the utilization of bis(imidazole) linkers (1,4-bib, 1,3-bib, 1,2-bimb) ligands as coligands to react with polycarboxylates was rarely reported in detail.[13] And the *cis*- or *trans*- configuration of bis(imidazole) linkers often causes the structural diversity when they coordinate to metal centers.[14]

Recent study on coordination assemblies by using 3,5-bis(3-carboxyphenyl)pyridine (H_2bcpb) and different N-donor ancillary ligands states a reliable strategy for obtaining new topological prototypes of coordination nets.[14e] Also, a minor change of the polycarboxylic acids building blocks may be applied to realize

[a] *State Key Laboratory of Crystal Materials, Shandong University , Jinan 250100, China. E-mail: zhaoxian@sdu.edu.cn.*
[b] *Advanced Material Institute of Research, College of Chemistry and Chemical Engineering, Qilu Normal University, Jinan, 250013, China. E-mail: xiutangzhang@163.com.*

†Electronic Supplementary Information (ESI) available: Additional figures, Powder XRD patterns, TG curves, and X-ray crystallographic data, CCDC 1046680-1046684 for **1-5**. See DOI: 10.1039/c5ra00000x.

good structural control of the resulted metal-organic polymers. Thus, these considerations inspired us to explore new coordination frameworks with designed 1,3-di(2',4'-dicarboxylphenyl)benzene (H_4DDB) ligand and different metal salts under solvothermal conditions in presence of bis(imidazole) linkers (shown in Scheme 1). In this paper, we reported the syntheses and characterizations of five novel coordination complexes, which exhibit systematic structural variation from 0D paddle wheel $\{Cu_2(COO)_4\}$ SBUs based complex (**4**), 1D $[Ni(H_2DDB)(H_2O)_2(\mu_2\text{-}H_2O)]_n$ chain (**1**), 3D 4-connected **cds** net (**5**), 3D (3,6)-connected $(3\cdot6\cdot7)(3^2\cdot4^3\cdot5^4\cdot6^3\cdot7\cdot8^2)$ net (**3**), to 3D (3,3,6)-connected $(6^3)_4(6^5\cdot8^8\cdot10^2)$ net (**2**). These results revealed that the H_4DDB ligand is a good candidate to construct inorganic building blocks based coordination complexes and the metal ions as well as the bis(imidazole) ancillary linkers have great influence on the final structures.

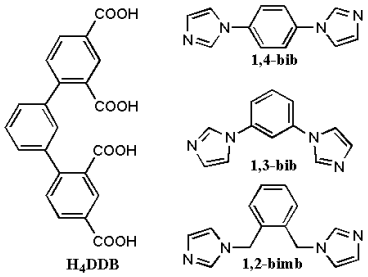

Scheme 1. The structure of H_4DDB and bis(imidazole) ancillary ligands.

Experimental Section

Reagents and Physical Measurements. All chemical reagents were purchased from Jinan Henghua Sci. & Tec. Co. Ltd. without further purification. Elemental analyses were carried out on a CE instruments EA 1110 elemental analyzer. TGA was measured from 25 to 800 °C on a SDT Q600 instrument at a heating rate 5 °C/min under the N_2 atmosphere (100 mL/min). X-ray powder diffractions were measured on a Panalytical X-Pert pro diffractometer with Cu-Kα radiation. The variable-temperature magnetic susceptibility measurements were performed on the Quantum Design SQUID MPMS XL-7 instruments in the temperature range of 2-300 K under a field of 1000 Oe. PXRD of **1**−**5** was measured and shown in Fig. S1. IR spectra were measured on a NEXUS 670 FTIR spectrometer in the range of 600-4000 cm^{-1} and given in Fig. S2.

Synthesis of $[Ni(H_2DDB)(H_2O)_2(\mu_2\text{-}H_2O)]_n$ (1). The mixture of H_4DDB (0.10 mmol, 0.041 g), $NiCl_2\cdot6H_2O$ (0.20 mmol, 0.048g), 6 mL H_2O, and 3 mL CH_3CN was sealed in the 25 mL Teflon-lined stainless steel vessel and heated to 130 °C for 5 days, and followed by slow cooling to room temperature at a descent rate of 10 °C/h. Green block crystals of **1** were obtained with the yield of 76% (based on H_4DDB). Anal. (%) calcd. for $C_{22}H_{18}NiO_{11}$: C, 51.10; H, 3.51. Found: C, 51.17; H, 3.67. IR (KBr pellet, cm^{-1}): 3225 (s), 2110 (w), 1686 (s), 1607 (m), 1547 (s), 1425 (m), 1367 (s), 1220 (s), 1164 (w), 1124 (s), 979 (w),896 (w), 792 (m), 767 (w), 669 (s), 623 (vs).

Synthesis of $[Ni_{1.5}(DDB)(1,4\text{-bib})_{1.5}(H_2O)]_n$ (2). The synthetic method is similar to that of complex **1** except that 1,4-bib (0.30 mmol, 0.063 g) was added as ancillary ligand. Green block crystals of **2** were obtained with the yield of 61% (based on H_4DDB). Anal. (%) calcd. for $C_{80}H_{56}N_{12}Ni_3O_{18}$: C, 58.32; H, 3.32; N, 10.20. Found: C, 58.47; H, 3.32; N, 10.41. IR (KBr pellet, cm^{-1}): 3363 (m), 3134 (s), 2113 (m), 1591 (vs), 1511 (vs), 1445 (m), 1378 (s), 1318 (m), 1281 (m), 1240 (m), 1065 (s), 1005 (w), 776 (m), 731 (m), 694 (m), 658 (m).

Synthesis of $\{[Ni_2(DDB)(1,3\text{-bib})_2(\mu_2\text{-}H_2O)]\cdot2H_2O\}_n$ (3). The synthetic method is similar to that of complex **1** except that the 1,3-bib (0.30 mmol, 0.063 g) was added as ancillary ligand. Green block crystals of **3** were obtained with the yield of 82% (based on H_4DDB). Anal. (%) calcd. for $C_{46}H_{34}N_8Ni_2O_{10}$: C, 56.60; H, 3.51; N, 11.48. Found: C, 56.72; H, 3.53; N, 11.50. IR (KBr pellet, cm^{-1}): 3457 (m), 31657 (m), 3138 (m), 1627 (m), 1603 (m), 1549 (s), 1524 (s), 1496 (m), 1448 (m), 1399 (m), 1367 (m), 1309 (s), 1065 (s), 826 (m), 776 (m), 734 (m), 653 (w).

Synthesis of $[Cu_2(H_2DDB)_2(1,4\text{-bib})_2]\cdot H_2O$ (4). The synthetic method is similar to that of complex **2** except that $CuSO_4\cdot5H_2O$ (0.20 mmol, 0.050g) replaced $NiCl_2\cdot6H_2O$ (0.20 mmol, 0.048g). Blue block crystals of **4** were obtained with the yield of 31% (based on H_4DDB). Anal. (%) calcd. for $C_{68}H_{44}Cu_2N_8O_{16}$: C, 60.22; H, 3.27; N, 8.26. Found: C, 60.61; H, 3.30; N, 8.42. IR (KBr pellet, cm^{-1}): 3186 (s), 2164 (m), 1686 (vs), 1607 (s), 1562 (m), 1546 (s), 1439 (m), 1422 (s), 1366 (vs), 1215 (s), 1163 (m), 1123 (s), 896 (m), 766 (s), 680 (m), 648 (w),.

Synthesis of $\{[Cu_{1.5}(HDDB)(1,2\text{-bimb})]\cdot H_2O\}_n$ (5). The synthetic method is similar to that of complex **4** except that 1,2-bib (0.30 mmol, 0.063 g) replaced 1,3-bib (0.30 mmol, 0.063 g). Purple blue crystals of **5** were obtained with the yield of 57% (based on H_4DDB). Anal. (%) calcd. for $C_{72}H_{54}Cu_3N_8O_{18}$: C, 57.27; H, 3.60; N, 7.42. Found: C, 57.47; H, 3.73; N, 7.38. IR (KBr pellet, cm^{-1}): 3124 (s), 2659 (m), 2116 (s), 1620 (s), 1525 (s), 1439 (m), 1403 (s), 1293 (m), 1240 (s), 1093 (s), 837 (s), 776 (m), 724 (s), 668 (m), 622 (vs).

X-ray crystallography. Intensity data collection was carried out on a Siemens SMART diffractometer equipped with a CCD detector using Mo-$K\alpha$ monochromatized radiation (λ = 0.71073 Å) at 296(2) K. The absorption correction was based on multiple and symmetry-equivalent reflections in the data set using the SADABS program based on the method of Blessing. The structures were solved by direct methods and refined by full-matrix least-squares using the SHELXTL package.[15] All non-hydrogen atoms were refined anisotropically. Hydrogen atoms except those for water molecules were generated geometrically with fixed isotropic thermal parameters, and included in the structure factor calculations. The approximate positions of the water H atoms, obtained from a difference Fourier map, were restrained to the ideal configuration of the water molecule and fixed in the final stages of refinement. Some carbon atoms and two nitrogen atoms of 1,3-bib in **3** and three lattice water molecules were refined with split positions and the occupancy ratio of 45.6 : 54.4 for C(13)-C(21) and N(6), 91.9 : 8.1 for C(4)-C(9), 88 : 12 for O(1W), and 37 : 13 for both O(2W) and O(3W). For complex **5**, five carbon atoms of 1,2-bimb and the lattice water molecule were refined with split positions and the occupancy ratio of 39 : 61 for C(28)-C(32) and 70.4 : 29.6 for O(1W). Crystallographic data and selected bond lengths and angles for complexes **1**–**5** are listed in Table 1 and Table S1. CCDC reference numbers: 1046680 for **1**, 1046681 for **2**, 1046682 for **3**,

1046683 for **4**, and 1046684 for **5**.

Table 1 Crystal data for **1–5**

Complex	**1**	**2**	**3**	**4**	**5**
Empirical formula	$C_{22}H_{18}NiO_{11}$	$C_{80}H_{56}N_{12}Ni_3O_{18}$	$C_{46}H_{36}N_8Ni_2O_{11}$	$C_{68}H_{48}Cu_2N_8O_{18}$	$C_{72}H_{54}Cu_3N_8O_{18}$
Formula weight	517.07	1649.50	994.25	1392.22	1509.85
Crystal system	Orthorhombic	Monoclinic	Monoclinic	Orthorhombic	Monoclinic
Space group	*Pnma*	$P2_1/n$	$C2/c$	*Pbca*	$P2_1/n$
a (Å)	7.7017(3)	12.2234(4)	42.0250(14)	19.4760(7)	17.8722(10)
b (Å)	22.7746(7)	10.2921(4)	11.1915(4)	10.5905(4)	10.9304(6)
c (Å)	11.5195(4)	28.1648(10)	23.6784(8)	29.7263(11)	19.1523(11)
α (°)	90	90	90	90	90
β (°)	90	98.6459(11)	120.5704(9)	90	115.5103(16)
γ (°)	90	90	90	90	90
V(Å^3)	2020.56(12)	3503.0(2)	9588.6(6)	6131.4(4)	3376.6(3)
Z	4	2	8	4	2
D_{calcd} (Mg/m^3)	1.700	1.564	1.377	1.508	1.485
μ(mm^{-1})	1.028	0.884	0.851	0.777	1.015
T(K)	296(2)	296(2)	296(2)	296(2)	296(2)
R_{int}	0.0408	0.0499	0.0542	0.0980	0.1415
θ range (°)	3.21–25.00	3.11–25.00	2.96–25.00	3.00–25.00	2.95–25.50
F(000)	1064	1696	4096	2856	1546
Data/restraints/parameters	1823/45/172	6155/3/517	8387/329/786	5382/0/485	6273/97/504
R indices (all data)	0.0290, 0.0506	0.0365, 0.0863	0.0602, 0.1274	0.0886, 0.1560	0.1161, 0.1078
Gof	1.051	1.000	1.064	1.057	1.046

$R_1 = \Sigma| |F_o|-|F_c| | / \Sigma|F_o|$, $wR_2 = [\Sigma w(F_o^2-F_c^2)^2]/ \Sigma w(F_o^2)^2]^{1/2}$

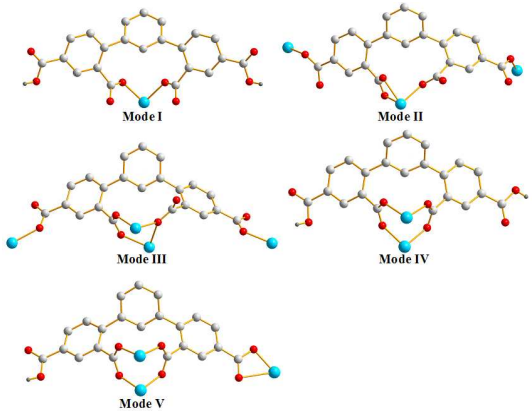

Scheme 2. The coordination modes of H_4DDB in complexes **1-5**.

Result and Discussion

Synthesis. Five title complexes were synthesized under hydrothermal conditions and their formation were strongly influenced by reaction conditions such as metal ions and ancillary linkers. The diverse coordination modes of H_4DDB proved that different bis(imidazole) linkers (1,4-bib, 1,3-bib, 1,2-bimb) also play an important role in adjusting the coordination mode of polycarboxylic acid and crystal packing structure.

Structural Description of $[Ni(H_2DDB)(H_2O)_2(\mu_2\text{-}H_2O)]_n$ (1). X-ray single-crystal determination reveals complex **1** possessed a three-dimensional supramolecular structure, built from 1D $[Ni(H_2O)_2(\mu_2\text{-}H_2O)]_n$ chains with the help of O–H···O hydrogen bonds. Complex **1** crystallizes in the orthorhombic system, space group *Pnma*. The asymmetric unit consists of half of Ni^{II} ion, half of H_2DDB^{2-} ligand, one and a half water molecules. In the building unit of **1**, the nickel center adopts a distorted octahedral geometry by coordinating to four water molecules and two oxygen atoms of two monodentate carboxyl groups from one H_2DDB^{2-}ligand (Fig. 1a). The bond lengths and angles of Ni-O are similar to those in other nickel-carboxylate coordination polymers.[16a-c] It is worth mentioning that the Ni-μ_2-OH_2 bond length is slightly longer than other five Ni-O ones.

In **1**, H_2DDB^{2-} is partly deprotonated and adopts the coordination mode of I, shown in Scheme 1. The two dihedral angles between the central phenyl ring and the two side phenyl rings are equal (49.3(4)°). And the dihedral angle between two side phenyl rings is 31.9(1)°. Two 2-position carboxyl groups were protonated and coordinated to one Ni^{II} cation. Furthermore, Ni^{II} ions are bridged by μ_2-coordinated water molecules to form 1D $[Ni(H_2O)_2(\mu_2\text{-}H_2O)]_n$ chain with the nearest Ni···Ni distance being 3.862 Å (Fig. 1b). Moreover, the neighbouring chains are interacted with each other through O–H···O hydrogen bonds (Table S2) to generate a 3D supramolecular structure (Fig. 1c).

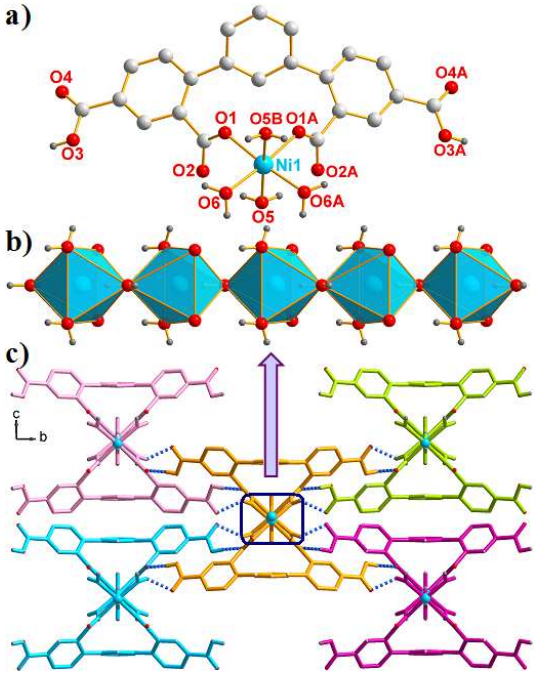

Figure 1. (a) Crystal structure of complex **1** (Symmetry codes: A: x, 3/2–y, z; B: 1/2+x, 3/2–y, 1/2–z.). (b) The 1D coordinated water molecules bridged $[Ni(H_2O)_2(\mu_2\text{-}H_2O)]_n$ chain. (c) Schematic view of the O-H···O hydrogen bonds based 3D supramolecular structure of **1** along a direction.

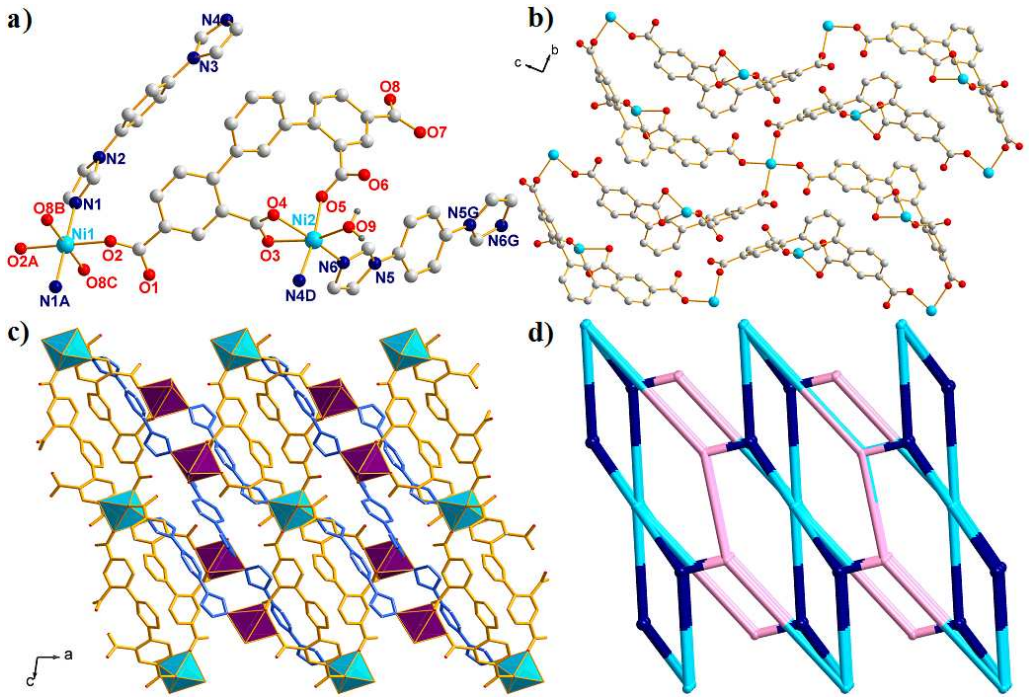

Figure 2. (a) Crystal structure of complex **2** (Symmetry codes: A: 2–*x*, 1–*y*, 1–*z*; B: 3/2–*x*, 1/2+*y*, 1/2–*z*; C: 1/2+*x*, 1/2–*y*, 1/2+*z*; D: 1+*x*, *y*, *z*; G: 2–*x*, –*y*, –*z*.). (b) The 2D $[Ni_3(DDB)_2]_n$ bilayer view along *a* direction. (c) Schematic view of the 3D frameworks of **2** along *b* direction. (d) The 3D novel (3,3.6)-connected $(6^3)_4(6^5{\cdot}8^8{\cdot}10^2)$ net of **2** (green nodes: Ni(1) ions, rose nodes: Ni(2) ions, dark blue nodes: DDB^{4-} ligands).

Structural Description of $[Ni_{1.5}(DDB)(1,4\text{-bib})_{1.5}(H_2O)]_n$ (2). X-ray crystallography reveals that **2** is a 3D $(6^3)_4(6^5{\cdot}8^8{\cdot}10^2)$ framework and crystallizes in the monoclinic system, space group $P2_1/n$. As shown in Fig. 2a, the asymmetric unit consists of one and a half Ni^{II} ions, one completely deprotonated DDB^{4-} ligand, one and a half 1,4-bib ligands, and one coordinated water molecule. Ni(1) is located in a slightly distorted $\{NiN_2O_4\}$ octahedral coordination environment, completed by four 4-position carboxyl groups from four distinct DDB^{4-} ligands, and two N atoms from two 1,4-bib ligands. Ni(2) is hexacoordinated by four O atoms from two 2-position carboxyl groups of one DDB^{4-} ligand and one coordinated water molecule, and two N atoms from two different 1,4-bib ligands, showing a distorted octahedral geometry. The Ni−O/N bond lengths are in the normal range of 2.0383(18)–2.1669(14) Å, respectively.[16d,e]

H_4DDB is completely deprotonated and adopts $(\kappa^1\text{-}\kappa^0)\text{-}(\kappa^1\text{-}\kappa^1)\text{-}(\kappa^1\text{-}\kappa^0)\text{-}(\kappa^1\text{-}\kappa^0)\text{-}\mu_3$ coordination mode (Mode II) to link three Ni^{II} ions. Ni(2) ions are cheated by monodentate 2-position carboxyl groups of DDB^{4-} ligands, which further connect Ni(1) ions *via* the terminal 4-position monodentate carboxyl groups to generate a 2D $[Ni_3(DDB)_2]_n$ bilayer (Fig. 2b). Moreover, Ni^{II} ions are linked by 1,4-bib linkers to construct a 1D $[Ni(1,4\text{-bib})]_n$ zigzag chain with Ni···Ni distances being 13.596 Å and 13.530 Å, in which 1,4-bib linkers adopted *trans*- configuration (Fig. S4). Finally, 1D $[Ni(1,4\text{-bib})]_n$ zigzag chains and 2D $[Ni_3(DDB)_2]_n$ bilayers are expanded to a 3D framework by sharing the Ni^{II} ions (Fig. 2c).

To better understand the final structure of complex **2**, the topology analysis was introduced to simplify the networks.[17] The final structure of **2** can be defined as an unprecedented (3,3,6)-connected net with the Schläfli symbol of $(6^3)_4(6^5{\cdot}8^8{\cdot}10^2)$ by denoting Ni(1) ions to 6–connected nodes, DDB^{4-} ligands and the Ni(2) ions to 3–connected nodes, respectively (Fig. 2d).

Structural Description of $\{[Ni_2(DDB)(1,3\text{-bib})_2(\mu_2\text{-}H_2O)]{\cdot}2H_2O\}_n$ (3). Sequentially, when we used 1,3-bib instead of 1,4-bib as the bridging co-ligand, $\{Ni_2(COO)(\mu_2\text{-}H_2O)\}$ SBUs based 3D (3,6)-connected $(3{\cdot}6{\cdot}7)(3^2{\cdot}4^3{\cdot}5^4{\cdot}6^3{\cdot}7{\cdot}8^2)$ net (**3**) was obtained. Complex **3** crystallizes in the monoclinic system *C*2/*c* and the asymmetric unit contains two Ni^{II} ions, one DDB^{4-} ligand, two 1,3-bib ligands, one μ_2- coordinated water molecule, and two lattice water molecules (Fig. 3a). Both Ni(1) and Ni(2) ions are located in distorted $\{NiN_2O_4\}$ octahedral coordination environments, surrounded by two oxygen atoms from two 2-position carboxylate groups of one DDB^{4-} ligand, one 4-position carboxylate oxygen atom form another DDB^{4-} ligand, one μ_2-H_2O molecule, and two nitrogen atoms from two 1,3-bib ligands. The Ni−N and Ni−O bond lengths are in the normal range of 2.057(3)–2.072(3) Å, and 2.050(2)–2.179(2) Å, respectively.

H_4DDB is completely deprotonated and adopts H_4DDB exhibits $(\kappa^1\text{-}\kappa^0)\text{-}(\kappa^1\text{-}\kappa^1)\text{-}(\kappa^2\text{-}\kappa^0)\text{-}(\kappa^1\text{-}\kappa^0)\text{-}\mu_4$ coordination mode (Mode III), different from that in complex **1** and **2**. Ni(1) and Ni(2) ions are connected by one μ_2-$\eta1$:$\eta1$-*syn-anti* 2-position carboxyl groups and one μ_2-H_2O molecule to form an unprecedented binuclear $\{Ni_2(COO)(\mu_2\text{-}H_2O)\}$ SBUs, which are further linked by 4-position carboxyl groups to generate a 2D sheet with opening area is about 11.192×26.839 $Å^2$ (Fig. 3b). From another point view, it is worth mentioning that four Ni^{II} ions are linked by four 1,3-bib to form an interesting $[Ni_4(1,3\text{-bib})_4]$ loop with the Ni···Ni distances being 9.532 and 11.430 Å, respectively (Fig. S5). And then $[Ni_4(1,3\text{-bib})_4]$ loops are hinged by adjacent 2D sheets to result in a 3D framework (Fig. 3c).

From the standpoint of topology, the final structure of **3** can be defined as a (3,6)-connected net with the Schläfli symbol of $(3{\cdot}6{\cdot}7)(3^2{\cdot}4^3{\cdot}5^4{\cdot}6^3{\cdot}7{\cdot}8^2)$ by denoting the DDB^{4-} ligands to 3–connected nodes, and the binuclear $\{Ni_2(COO)(\mu_2\text{-}H_2O)\}$ SBUs to 6–connected nodes, respectively (Fig. 3d).

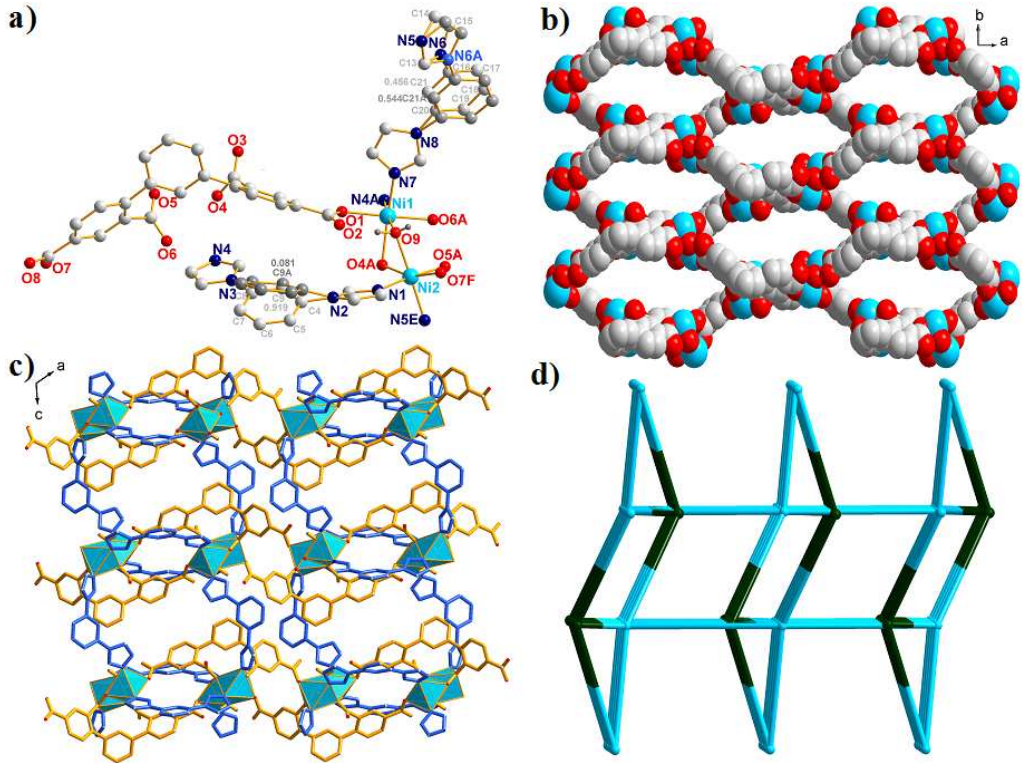

Figure 3. (a) Crystal structure of complex **3** (Symmetry codes: A: 2–*x*, 1–*y*,–*z*; E: *x*, 1–*y*, –1/2+*z*; F: 1/2+*x*, 3/2+*y*, 1/2+*z*.). (b) The space-filling of 2D $[Ni_2(DDB)(\mu_2\text{-}H_2O)]_n$ networks view along *c* direction. (c) Schematic view of the 3D frameworks of **3** along *b* direction. (d) The unprecedented binuclear $\{Ni_2(COO)(\mu_2\text{-}H_2O)\}$ SBUs based 3D (3,6)-connected $(3\cdot6\cdot7)(3^2\cdot4^3\cdot5^4\cdot6^3\cdot7\cdot8^2)$ net of **3** (green spheres: binuclear $\{Ni_2(COO)(\mu_2\text{-}H_2O)\}$ clusters based SBUs; dark green spheres: DDB^{4-} ligands).

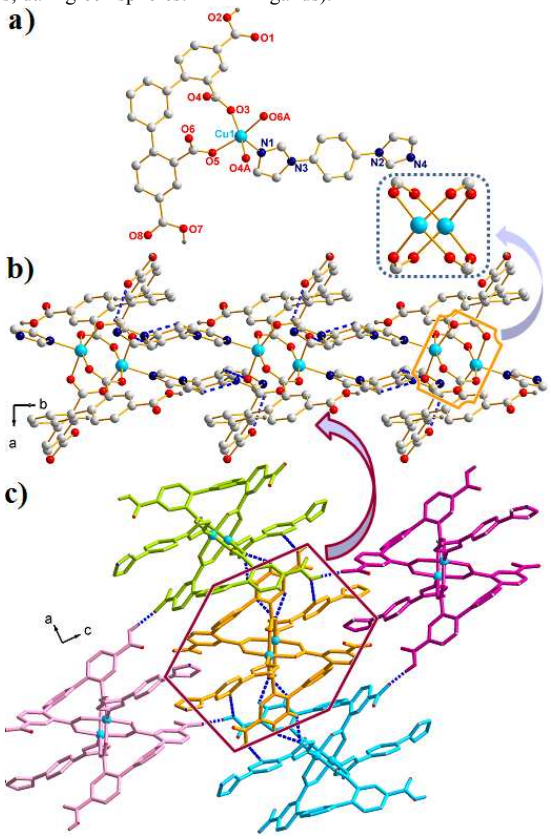

Figure 4. (a) Crystal structure of complex **4** (Symmetry code: A: 1–*x*, 2–*y*, 1–*z*.). (b) Schematic view of hydeogen bonds based 1D chain and (c) 3D supramolecular structure of **4**.

Structural Description of $[Cu_2(H_2DDB)_2(1,4\text{-bib})_2]\cdot H_2O$ (4). Although the reaction condition is similar with that in complex **2**, the final packing diagram of **4** exhibited an entirely different 0D paddle wheel $\{Cu_2(COO)_4\}$ SBUs based complex, which may be attributed to the different coordination preferences between Cu^{II} and Ni^{II} cations. Structural analysis reveals that complex **4** crystallizes in the orthorhombic system, space group *Pnca*.

As shown in Fig. 4a, there are one crystallographically independent Cu^{II} ion, one H_2DDB^{2-} ligand, and one 1,4-bib ligand in the asymmetric unit. Each Cu^{II} centre is pentacoordinated by four 2-position carboxylate groups from two H_2DDB^{2-} ligands and one N atom from 1,4-bib ligand, exhibiting a distorted square pyramid coordination geometry. In the paddle wheel $\{Cu_2(COO)_4\}$ SBUs, the Cu···Cu distance is 2.778 (8) Å. The dihedral angles between two side phenyl rings and central phenyl ring in H_2DDB^{2-} are 43.9(4) and 42.2(2)°, respectively. And the one between two side phenyl rings is 48.6(7)°. $\{Cu_2(COO)_4\}$ SBUs are interacted with each other *via* C–H···O hydrogen bonds [C(27)–H(27)···O(4)$^{\#1}$ = 3.436 Å, C(24)–H(24)···O(4)$^{\#1}$ = 3.632 Å, Symmetry code: #1 *x*, *y*–1, *z*.] to form a 1D chains along *c* axis (Fig. 4b), which are further linked by O–H···O/N hydrogen bonds [O(2)–H(2)···O(8)$^{\#2}$ = 2.638 Å, O(7)–H(7)A···N(4)$^{\#3}$ = 2.638 Å, Symmetry codes: #2 –*x*+3/2, –*y*+2, –*z*+1/2; #3 *x*, –*y*+1/2, *z*–1/2.] to generate a 3D supramolecular structure (Fig. 4c). And the detail hydrogen bonds are listed in Table S3.

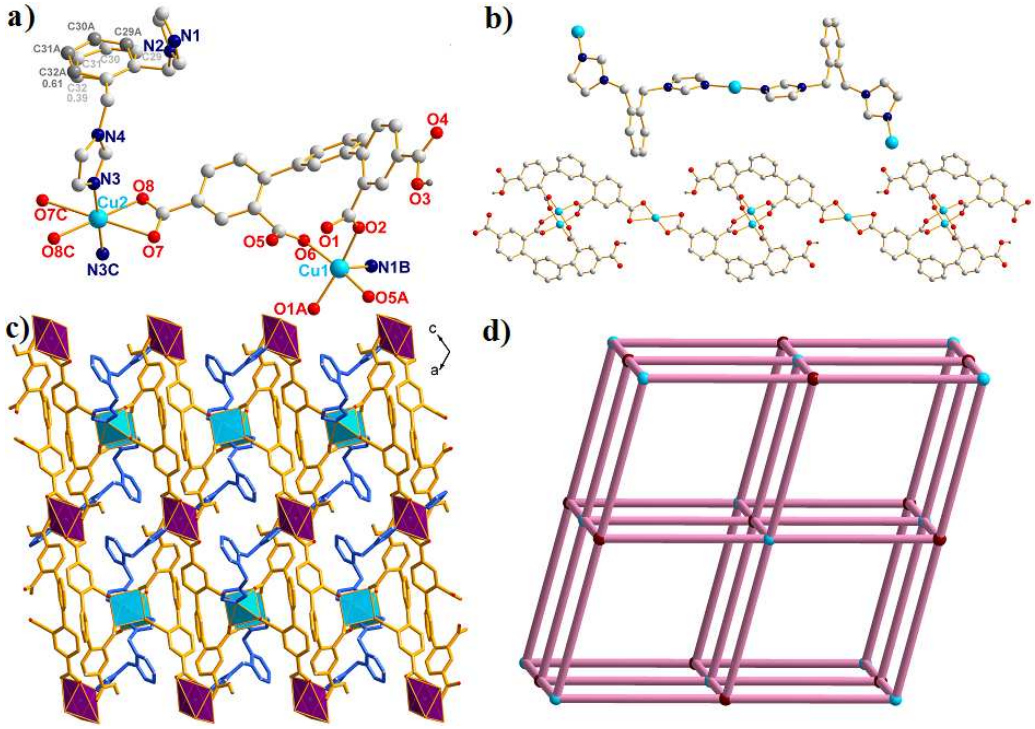

Figure 5. (a) Crystal structure of complex **5** (Symmetry codes: A: 1–*x*, 1–*y*, 2–*z*; B: 1/2–*x*, –1/2+*y*, 3/2–*z*; C: 1–*x*, 1–*y*, 1–*z*.). (b) The $[Cu_3(1,2\text{-bimb})_2]$ (the above) and the 1D $[Cu_3(HDDB)_2]_n$ chain (the below). (c) Schematic view of the 3D frameworks of **5** along *b* direction. (d) The 3D 4–connected $(6^5{\cdot}8)$-**cds** net of **5** (green nodes: paddle wheel $\{Cu_2(COO)_4\}$ SBUs, dark red nodes: Cu(2) ions).

Table 2 The detailed comparisons of complexes **1**–**5**.

Complex	Coordination Modes	Ancillary Ligands/Role	Dihedral Angles (°) of H_xDDB	Final Structure and Topology
1	Mode I	N/A	49.3(4)/31.9(1)/49.3(4)	1D water bridged Ni-H_2O chain
2	Mode II	1,4-bib/bridging	32.9(4)/59.8(7)/60.5(7)	3D (3,3.6)-connected $(6^3)_4(6^5{\cdot}8^8{\cdot}10^2)$ net
3	Mode III	1,3-bib/bridging	41.0(3)/53.8(3)/64.0(8)	3D (3,6)-connected $(3{\cdot}6{\cdot}7)(3^2{\cdot}4^3{\cdot}5^4{\cdot}6^3{\cdot}7{\cdot}8^2)$ net
4	Mode IV	1,4-bib/bridging	43.9(4)/48.6(7)/43.2(2)	0D supramolecular structure
5	Mode V	1,2-bimb/bridging	51.4(9)/42.7(8)/46.6(1)	3D 4–connected $(6^5{\cdot}8)$-**cds** net

Structural Description of $\{[Cu_{1.5}(HDDB)(1,2\text{-bimb})]\cdot H_2O\}_n$ (5). Structural analysis reveals that complex **5** crystallizes in the monoclinic system $P2_1/n$. There are one and a half crystallographically independent Cu^{II} ions, one $HDDB^{3-}$ ligand, one 1,2-bimb ligand, and one lattice water molecule in the asymmetric unit (Fig. 5a). Cu(1) is pentacoordinated by four 2-position carboxylate groups from two $HDDB^{3-}$ ligands and one N atom from 1,2-bib ligand, showing a distorted square pyramid coordination environment. While Cu(2) ions are surrounded by four O atoms from two distinct $HDDB^{3-}$ ligands and two N atoms from two 1,2-bimb ligands, showing a distorted $\{CuO_4N_2\}$ octahedral coordination geometry.

The ligand of H_4DDB is partly deprotonated and acts as μ_3 node to coordinate with three Cu^{II} ions, in which 2-position and 4-position carboxylate groups adopt syn-syn μ_2-η^1:η^1 and μ_1-η^1:η^0 coordination modes, respectively (Mode V). Two Cu(1) ions are connected by four μ_2-η^1:η^1 carboxyl groups to form a binuclear paddle wheel $\{Cu_2(COO)_4\}$ SBUs with the nearest Cu(1)···Cu(1) distance being 2.692 (8) Å, which are further bridged by two 4-position carboxylate groups from two other neighbour SBUs SBUs to form a 1D $[Cu_3(HDDB)_2]_n$ chain (Fig. 5b). Meanwhile, 1,2-bimb ligands expanded those 1D $[Cu_3(HDDB)_2]_n$ chains to generate a 3D framework by connecting the $\{Cu_2(COO)_4\}$ SBUs and Cu(2) ions alternately (Fig. 5c).

From a topological perspective, $\{Cu_2(COO)_4\}$ SBUs and Cu(2) ions act as 3-connected and 4-connected nodes, respectively, giving rise to a 3D 4–connected $(6^5{\cdot}8)$-**cds** net (Fig. 5d).

Structural Comparison and Discussion. As shown in Scheme 1 and Table 2, H_4DDB exhibits versatile coordination modes including $((\kappa^1\text{-}\kappa^0)\text{-}(\kappa^1\text{-}\kappa^0)\text{-}\mu_1$ (Mode I, in **1**), $(\kappa^1\text{-}\kappa^0)\text{-}(\kappa^1\text{-}\kappa^1)\text{-}(\kappa^1\text{-}\kappa^0)\text{-}(\kappa^1\text{-}\kappa^0)\text{-}\mu_3$ (Mode II, in 2), $(\kappa^1\text{-}\kappa^0)\text{-}(\kappa^1\text{-}\kappa^1)\text{-}(\kappa^2\text{-}\kappa^0)\text{-}(\kappa^1\text{-}\kappa^0)\text{-}\mu_4$ (Mode III, in 3), $(\kappa^1\text{-}\kappa^1)\text{-}(\kappa^1\text{-}\kappa^1)\text{-}\mu_2$ (Mode IV, in 4), and $(\kappa^1\text{-}\kappa^1)\text{-}(\kappa^1\text{-}\kappa^1)\text{-}(\kappa^1\text{-}\kappa^1)\text{-}\mu_3$ (Mode V, in 5)). The H_4DDB ligands act as μ_1- to μ_4-linkers to connect the transition metal centers, giving 0D paddle wheel $\{Cu_2(COO)_4\}$ SBUs to 3D frameworks, which further interact with the ancillary ligands or hydrogen bonds, leaving the 3D high-connected frameworks. This proved the fact that the subtle assembled progress is influenced by many intrinsic and external parameters, such as the different coordination preferences of metal ion as well as number of coordination sites provided by organic ligands. Meanwhile, this also illustrated that the carboxyl groups fixed in different phenyl position have different coordination ability to metal ions. It is also woth noting that the further linkage *via* the auxiliary ligands with different configurations could result in novel intere

Thermal Analyses. The thermogravimetric analyses (TGA) have been performed on the samples of **1**–**5** under N_2 atmosphere and TG curves were shown in Fig. S6. Complex **1** loses coordinated water molecules gradually (obsd. 6.8%, calcd. 6.9%)

before 140 °C, and then starts to lose its ligands. There are two main weight losses in the thermal decomposition process of **2**, the first weight loss of 2.4 % in the range of 75-120 °C is quite consistent with the release of coordinated water molecules (2.2 %); after that, an abrupt weight loss up to 330 °C corresponds to the loss of the organic ligands. For **3**, the weight loss of 5.36 % from 70 to 190°C is attributed to the loss of coordinated and lattice water molecules (calc. 5.45 %). And then the network began to collapse with the release of organic ligands. For **4**, the weight loss was found from the room temperature to 140 °C, corresponding to the dehydration process. Upon further heating, the second weight loss appeared, which was attributed to the decomposition of H_2DDB^{2-} and 1,4-bib ligands. For 5, the first weight loss was measured to be 2.46 % which appears from the room temperature to 105 °C, corresponding to the dehydration process (cacld. 2.38 %). Upon further heating, the second weight loss took place due to the decomposition of the organic ligands.

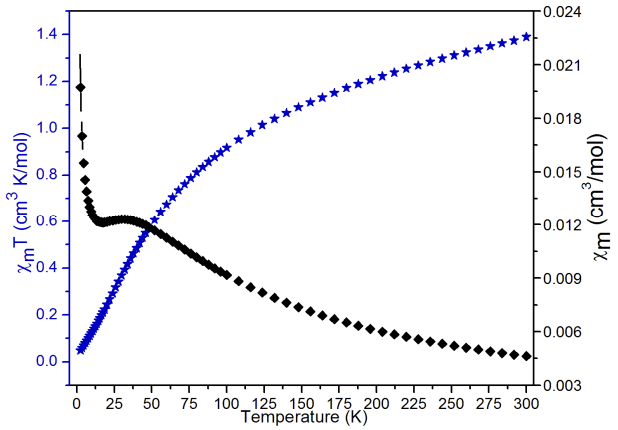

Figure 6. The temperature dependence of magnetic susceptibility of **1** under a static field of 1000 Oe.

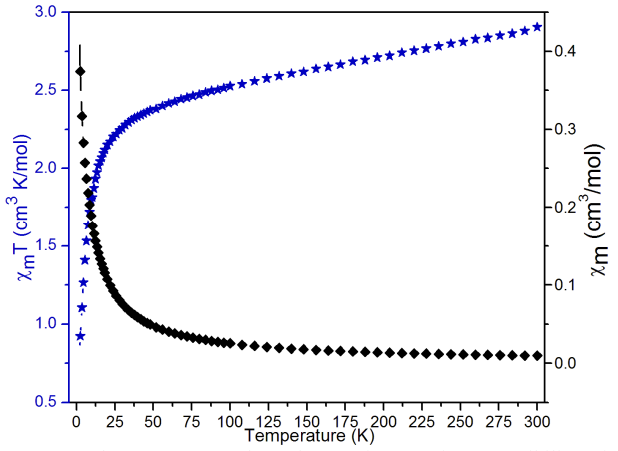

Figure 7. The temperature dependence of magnetic susceptibility of **3** under a static field of 1000 Oe.

Magnetic Properties. The variable-temperature magnetic susceptibility measurements of **1**, **3**, and **5** were investigated and discussed below. As shown in Fig. 6, the $\chi_M T$ value of **1** is 1.39 cm^3 K mol^{-1} at room temperature, larger than the expected value for one isolated Ni^{II} ion (S=1) (1.05 cm^3 K mol^{-1}) and much lower than two isolated ones (2.10 cm^3 K mol^{-1}), consistent with the reported $[Ni(\mu_2\text{-}H_2O)]_n$ chain. With the temperature decreasing, the $\chi_M T$ value decreases continuously to 0.04 cm^3 K mol^{-1} at about 2K. Meanwhile, the temperature dependence χ_M followed the Curie-Weiss law $\chi_M = C/(T-\theta)$ with C= 1.87 cm^3 K mol^{-1}, θ= –107.75 K (Fig. S7). The curve of χ_MT at 2K~300K and the θ value indicates that complex **1** shown antiferromagnetic property.[18a-c] For complex **3** (Fig. 7), the χ_MT value at room temperature is 2.91 cm^3 K mol^{-1}, larger than that for two magnetically isolated Ni^{II} ions (2.1 cm^3 K mol^{-1}), which can be attributed to the contribution of the susceptibility from orbital angular momentum at higher temperature. With the temperature decreasing, the $\chi_M T$ value decreases continuously to 0.83 cm^3 K mol^{-1} at about 2K. The temperature dependence χ_M followed the Curie-Weiss law $\chi_M = C/(T-\theta)$ with C= 3.18 cm^3 K mol^{-1}, θ= –29.78 K (Fig. S8). And the negative value of θ also indicates complex **3** aslo owns the antiferromagnetic property.[18d,e] For **5**, the χ_MT value at room temperature is 1.32 cm^3 K mol^{-1}, and then the χ_MT value steadily decreases with the temperature decreasing, reaching a minimum value of 0.86 cm^3 at 59K (Fig. 8). Upon further cooling, the $\chi_M T$ value increase up to a maximum of 1.54 cm^3 K mol^{-1} at about 2K. The increase of $\chi_M T$ value between 60 and 300 K is due to the antiferromagnetic behaviour of the neighbouring Cu^{II} ions. And the $\chi_M T$ decrease at low temperature reveals a strong ferromagnetic coupling between the adjacent units. [19]

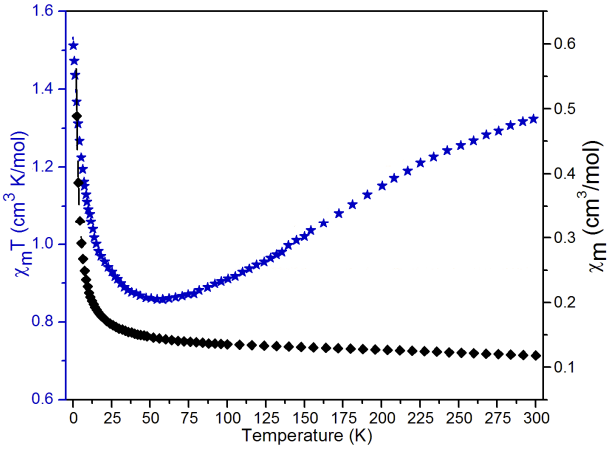

Figure 8. The temperature dependence of magnetic susceptibility of **5** under a static field of 1000 Oe.

Conclusions

In summary, five new complexes based on 1,3-di(2',4'-dicarboxylphenyl)benzene (H_4DDB) ligand and bis(imidazole) linkers have been successfully synthesized under solvothermal conditions. Compounds **1**–**5** displayed appealing structural features from 0D paddle wheel $\{Cu_2(COO)_4\}$ SBUs to 3D frameworks, such as the novel unprecedented 3D (3,3,6)-connected $(6^3)_4(6^5\cdot8^8\cdot10^2)$ host-framework of **2** and the 3D (3,6)-connected $(3\cdot6\cdot7)(3^2\cdot4^3\cdot5^4\cdot6^3\cdot7\cdot8^2)$ network of **3**. A structural comparison of these networks reveals that H_4DDB is an effective ligand with rich coordination modes, which is useful to better understand the synthon selectivity in multifunctional crystal structures. In addition, the employment of the bis(imidazole) bridging ligands during the assembly of the metal–polycarboxylate system often leads to structural changes and affords new frameworks. The variable-temperature magnetic

susceptibility measurements exhibit that complexes of **1** and **3** own the antiferromagnetic property, and complex of **5** shows ferromagnetic property.

Acknowledgements. The work was supported by financial support from the Natural Science Foundation of China (Grant Nos. 21101097, 21451001), key discipline and innovation team of Qilu Normal University.

Notes

The authors declare no competing financial interest.

References

1. (a) G. Férey and C. Serre, *Chem. Soc. Rev*., 2009, **38**, 1380; (b) Z. H. Wang, D. F. Wang, T. Zhang, R. B. Huang and L. S. Zheng, *CrystEngComm*, 2014, **16**, 5028; (c) M. Zhang, W. Lu, J. R. Li, M. Bosch, Y. P. Chen, T. F. Liu, Y. Liu and H. C. Zhou, *Inong. Chem. Front.*, 2014, **1**, 159; (d) W. Shi, S. Song and H. Zhang, *Chem. Soc. Rev*., 2013, **42**, 5714; (e) K. Wang, S. Zeng, H. Wang, J. Dou and J. Jiang, *Inong. Chem. Front.*, 2014, **1**, 167; (f) W. L. Leong and J. J.Vittal, *Chem. Rev.*, 2011, **111**, 688.
2. (a) T. R. Cook, Y. R. Zheng and P. J. Stang, J. *Chem. Rev.*, 2013, **113**, 734; (b) B. L. Chen, N. W. Ockwig, A. R. Millward, D. S. Contreras and O. M. Yaghi, *Angew. Chem. Int. Ed*., 2005, **44**, 4745; (c) M. Kim, J. F. Cahill, H. Fei, K. A. Prather and S. M. Cohen, *J. Am. Chem. Soc*., 2012, **134**, 18082; (d) S. L. Huang, A. Q. Jia and G. X. Jin, *Chem. Commun.*, 2013, **49**, 2403; (e) D. S. Li, Y. P. Wu, J. Zhao, J. Zhang and J. Y. Lu, *Coord. Chem. Rev*., 2014, **261**, 1.
3. (a) E. D. Bloch, W. L. Queen, R. Krishna, J. M. Zadrozny, C. M. Brown and J. R. Long, *Science*, 2012, **335**, 1606; (b) S. Chen, R. Shang, K. L. Hu, Z. M. Wang and S. Gao, *Inong. Chem. Front.*, 2014, **1**, 83; (c) X. T. Zhang, D. Sun, B. Li, L. M. Fan, B. Li and P. H. Wei, *Cryst. Growth Des.*, 2012, **12**, 3845; (d) X. J. Kong, Y. Wu, L. S. Long, L. S. Zheng and Z. Zheng, *J. Am. Chem. Soc*., 2009, **131**, 6918; (e) W. Liu, X. Bao, L. L. Mao, J. Tucek, R. Zboril, J. L. Liu, F. S. Guo, Z. P. Ni and M. L. Tong, *Chem. Commun.*, 2014, **50**, 4059; (f) S. L. Huang, Y. J. Lin, T. S. A. Hor and G. X. Jin, *J. Am. Chem. Soc*., 2013, **135**, 8125.
4. (a) T. Wu, Y. J. Lin and G. X. Jin, *Dalton Trans.*, 2014, **43**, 2356; (b) X. T. Zhang, L. M. Fan, X. Zhao, D. Sun, D. C. Li and J. M. Dou, *CrystEngComm*, 2012, **14**, 2053; (c) J. J. Liu, Y. J. Lin and G. X. Jin, *Organometallics,* 2014, **33**, 1283; (d) J. B. Lin, W. Xue, B. Y. Wang, J. Tao, W. X. Zhang, J. P. Zhang and X. M. Chen, *Inorg. Chem*., 2012, **51**, 9423; (e) X. Zhang, L. Fan, W. Zhang, Y. Ding, W. Fan and X. Zhao, *Dalton Trans.,* 2013, **42**, 16562; (f) H. Li, Y. F. Han, Y. J. Lin, Z. W. Guo and G. X. Jin, *J. Am. Chem. Soc*., 2014, **136**, 2982.
5. (a) R. Pedrido, M. Vázquez López, L. Sorace, A. M. González-Noya, M. Cwiklinska, Vanesa Suárez-Gómez, G. Zaragozad and M. R. Bermejoa, *Chem. Commun.*, 2010, **46**, 4797; (b) C. Zhan, C. Zou, G. Q. Kong and C. D. Wu, *Cryst. Growth Des.*, 2013, **13**, 1429; (c) X. Chang, Y. Zhao, M. Han, L. Ma and L. Wang, *CrystEngComm*, 2014, **16**, 6417; (d) D. S. Li, X. J. Ke, J. Zhao, M. Du, K. Zou, Q. F. He and C. Li, *CrystEngComm*, 2011, **13**, 3355; (e) M. Meng, D. C. Zhong and T. B. Lu, *CrystEngComm*, 2011, **13**, 6794.
6. (a) U. J. Williams, B. D. Mahoney, A. J. Lewis, P. T. DeGregorio, P. J. Carroll and E. J. Schelter, *Inorg. Chem.*, 2013, **52**, 4142; (b) T. Liu, S. Wang, J. Lu, J. Dou, M. Niu, D. Li and J. Bai, *CrystEngComm*, 2013, **15**, 5476; (c) Y. W. Li, D. C. Li, J. Xu, H. G. Hao, S. N. Wang, J. M. Dou, T. L. Hu and X. H. Bu, *Dalton Trans.,* 2014, **43**, 15708; (d) H. Deng, S. Grunder, K. E. Cordova, H. Furukawa, M. Hmadeh, F. Gandara, A. C. Whalley, Z. Liu, S. Asahina, H. Kazumori, M. O'Keefee, O. Terasaki, J. F. Stoddart and O. M. Yaghi, *Science*, 2012, **336**, 1018.
7. (a) R. E. Osta, M. Frigoli, J. Marrot, N. Guillou, H. Chevreau, R. I. Walton and F. Millange, *Chem. Comm.*, 2012, **48**, 10639; (b) J. Zhao, D. S. Li, X. J. Ke, B. Liu, K. Zou and H. M. Hu, *Dalton Trans.,* 2012, **41**, 2560; (c) W. Liu, L. Ye, X. Liu, L. Yuan, J. Jiang and C. Yan, *CrystEngComm*, 2008, **10**, 1395; (d) M. Yan, F. Jiang, Q. Chen, Y. Zhou, R. Feng, K. Xiong and C. Hong, *CrystEngComm*, 2011, **13**, 3971; (e) X. S. Wang, S. Ma, K. Rauch, J. M. Simmons, D. Yuan, X. Wang, T. Yildirim, W. C. Cole, J. J. Lopez, A. de Meijere and H. C. Zhou, *Chem. Mater.*, 2008, **20**, 3145; (f) M. D. Zhang, Z. Q. Shi, M. D. Chen and H. G. Zheng, *Dalton Trans.,* 2015, **44**, 5818.
8. (a) J. L. Liu, Y. C. Chen, Y. Z. Zheng, W. Q. Lin, L. Ungur, W. Wernsdorfer, L. F. Chibotaru and M. L. Tong, *Chem. Sci.*, 2013, **4**, 3310; (b) X. H. Chang, Y. Zhao, M. L. Han, L. F. Ma and L. Y. Wang, *CrystEngComm*, 2014, **16**, 6417; (c) L. P. Xue, C. X. Chang, S. H. Li, L. F. Ma and L. Y. Wang, *Dalton Trans.,* 2014, **43**, 7219; (d) M. L. Han, X. C. Chang, X. Feng, L. F. Ma and L. Y. Wang, *CrystEngComm*, 2014, **16**, 1687; (e) L. L. Liu, C. X. Yu, J. Sun, P. P. Meng, F. J. Ma, J. M. Du and L. F. Ma, *Dalton Trans.,* 2014, **43**, 2915; (f) T. Wang, C. Zhang, Z. Ju and H. Zheng, *Dalton Trans.,* 2015, **44**, 6926.
9. (a) L. Liu, X. Lv, L. Zhang, L. Guo, J. Wu, H. Hou and Y. Fan, *CrystEngComm*, 2014, **16**, 8736; (b) G. Yu, N, Y, Li, X. Y. Ji, J. F. Wang, D. Liu and X. Y. Tang, *CrystEngComm*, 2014, **16**, 6621; (c) X. C. Yi, M. X. Huang, Y. Qi and E. Q. Gao, *Dalton Trans.,* 2014, **43**, 3691; (d) J. Yang, X. Wang, F. Dai, L. Zhang, R. Wang and D. Sun, *Inorg. Chem.,* 2014, **53**, 10649; (e) H. Jia, Y. Li, Z. Xiong, C. Wang and G. Li, *Dalton Trans.,* 2014, **43**, 3704; (f) J. Cui, Y. Li, Z. Guo and H. Zheng, *Chem. Commun.*, 2013, **49**, 555.
10. (a) L. Fan, W. Fan, W. Song, G. Liu, X. Zhang and X. Zhao, *CrystEngComm*, 2014, **16**, 9191; (b) X. Zhang, L. Fan, Z. Sun, W. Zhang, W. Fan, L. Sun and X. Zhao, *CrystEngComm*, 2013, **15**, 4910; (c) X. Q. Song, Y. K. Lei, X. R. Wang, M. M. Zhao, Y. Q. Peng and G. Q. Cheng, *J. Solid State Chem.*, 2014, **210**, 178; (d) X. Song, Z. Xiao, M. Zhao and W. Qian, *Z. anorg. allg. Chem.*, 2014, **640**, 1769.
11. (a) Y. Q. Chen, S. J. Liu, Y. W. Li, G. R. Li, K. H. He, Z. Chang and X. H. B, *CrystEngComm*, 2013, **15**, 1613; (b) T. Cao, Y. Peng, T. Liu, S. Wang, J. Dou, Y. Li, C. Zhou, D. Li and J. Bai, *CrystEngComm*, 2014, **16**, 10658; (c) L. Zhang, J. Guo, Q. Meng, R. Wang and D. Sun, *CrystEngComm*, 2013, **15**, 9578; (d) Z. H. Yan, X. W. Zhang, H. Pang, Y. Zhang, D. Sun and L. Wang, *RSC Adv.*, 2014, **4**, 53608; (e) F. Y. Yi, S. Dang, W. Yan and Z. M. Sun, *CrystEngComm*, 2013, **15**, 8320; (f) L. Fan, W. Fan, B. Li, X. Liu, X. Zhao and X. Zhang, *Dalton Trans.*, 2015, **44**, 2380.
12. (a) X. H. Chang, J. H. Qin, M. L. Han, L. F. Ma and L. Y. Wang, *CrystEngComm*, 2014, **16**, 8720; (b) L. Fan, X. Zhang, W. Zhang, Y. Ding, W. Fan, L. Sun, Y. Pang and X. Zhao, *Dalton Trans.,* 2014, **43**, 6701; (c) X. Zhang, L. Fan, W. Zhang, W. Fan, L. Sun and X. Zhao, *CrystEngComm*, 2014, **16**, 3203; (d) L. Fan, Y. Gao, G. Liu, W. Fan, W. Song, L. Sun, X. Zhao and X. Zhang, *CrystEngComm*, 2014, **16**, 7649; (e) W. Yang, C. Yang, Q. Ma, C. Li, H. Wang and J. Jiang, *CrystEngComm*, 2014, **16**, 4554;.
13. (a) Z. Wu, W. Sun, Y. Chai, W. Zhao, H. Wu, T. Shi and X. Yang, *CrystEngComm*, 2014, **16**, 406; (b) F. Guo, B. Zhu, M. Liu, X. Zhang, J. Zhang and J. Zhao, *CrystEngComm*, 2013, **15**, 6191; (c) L. Chen, L. Zhang, S. L. Li, Y. Q. Qiu, K. Z. Shao, X. L. Wang and Z. M. Su, *CrystEngComm*, 2013, **15**, 8214; (d) X. Zhang, L. Fan, W. Song, W. Fan, L. Sun and X. Zhao, *RSC Adv.*, 2014, **4**, 30274; (e) L. Fan, W. Fan, B. Li, X. Liu, X. Zhao and X. Zhang, *RSC Adv.*, 2015, 2015, **5**, 14897.
14. (a) L. Fan, W. Fan, W. Song, L. Sun, X. Zhao and X. Zhang, *Dalton Trans.,* 2014, **43**, 15979; (b) L. Fan, X. Zhang, Z. Sun, W. Zhang, Y. Ding, W. Fan, L. Sun, X. Zhao and H. Lei, *Cryst. Growth Des.*, 2013, **13**, 2462; (c) X. T. Zhang, L. M. Fan, Z. Sun, W. Zhang, D. C. Li, J. M. Dou and L. Han, *Cryst. Growth Des*., 2013, **13**, 792; (d) T. Wu, Y. J. Lin and G. X. Jin, *Dalton Trans.*, 2014, **42**, 82; (e) L. Fan, X. Zhang, W. Zhang, Y. Ding, L. Sun, W. Fan and X. Zhao, *CrystEngComm*, 2014, **16**, 2144.
15. (a) G. M. Sheldrick, *SHELXTL*, version 5.1; Bruker Analytical X-ray Instruments Inc.: Madison, WI, 1998. (b) G. M. Sheldrick, *SHELX-97*, PC Version; University of Gottingen: Gottingen, Germany, 1997.
16. (a) H. S. Jena, S. Goswami, S. Snada, S. Parshamoni, S. Biswas and S. Konar, *Dalton Trans.,* 2014, **43**, 16996; (b) S. D. Liu, B. C. Kuo,

Y. W. Liu, J. Y. Lee, K. W. Wong and H. M. Lee, *CrystEngComm*, 2014, **16**, 8874; (c) F. Su, L. Lu, S. Feng and M. Zhu, *Dalton Trans.,* 2014, **43**, 7990; (d) J. W. Lin, P. Thanasekaran, J. S. Chang, J. Y. Wu, L. L. Lai and K. L. Lu, *CrystEngComm*, 2013, **15**, 9798; (e) F. L. Hu, Y. Mi, Y. Q. Guo, L. G. Zhu, S. L. Yang, H. Wei and J. P. Lang, *CrystEngComm*, 2013, **15**, 9553.

17. (a) V. A. Blatov, A. P. Shevchenko and V. N. Serezhkin, *J. Appl. Crystallogr.*, 2000, **33**, 1193; (b) The network topology was evaluated by the program "TOPOS-4.0", see: http://www.topos.ssu.samara.ru. (c) V. A. Blatov, M. O'Keeffe and D. M. Proserpio, *CrystEngComm*, 2010, **12**, 44.

18. (a) S. K. Lee, K. W. Tan and S. W. Ng, *RSC Adv.*, 2014, **4**, 60280; (b) Y. H. Cui, J. Wu, A. M. Kirillov, J. Z. Gu and W. Dou, *RSC Adv.*, 2015, **5**, 10400; (c) J. Z. Qiao, M. S. Zhan and T. P. Hu, *RSC Adv.*, 2014, **4**, 62285; (d) K. Ohno, A. Nagasawa and T. Fujihara, *Dalton Trans.,* 2015, **44**, 368; (e) Y. Y. Yang, Z. J. Lin, T. T. Liu, J. Liang and R. Cao, *CrystEngComm*, 2015, **17**, 1381.

19. (a) B. Shen, P. F. Shi, Y. L. Hou, F. F. Wan, D. L. Gao and B. Zhao, *Dalton Trans.,* 2013, **42**, 3455; (b) Y. Pang, D. Tian, X. F. Zhu, Y. H. Luo, X. Zheng and H. Zhang, *CrystEngComm*, 2011, **13**, 5142; (c) L. F. Ma, J. W. Zhao, M. L. Han, L. Y. Wang and M. Du, *Dalton Trans.,* 2012, **41**, 2078.

RSC Advances

For Table of Contents Use Only

Table of Contents Graphic and Synopsis

Hydrothermal Syntheses, Structural Characterizations, and Magnetic Properties of Five MOFs Assembled From C_2-Symmetric Ligand of 1,3-Di((2',4'-dicarboxylphenyl)benzene with Various Coordination Modes

Liming Fan, Weiliu Fan, Bin Li, Xian Zhao and Xiutang Zhang

Five new complexes with appealing structural features from 0D paddle wheel $\{Cu_2(COO)_4\}$ SBUs to 3D frameworks were reported to better understand the synthon selectivity in multifunctional crystal structures.